14

Finite Element Analysis of Nonlinear Isotropic Hyperelastic and Viscoelastic Materials for Thermoforming Applications

Erchiqui Fouad
Université du Québec an Abitibi-Témiscamingue
Rouyn-Noranda, Québec
Canada

1. Introduction

Thermoforming of cut sheets is extensively used in the industry for various commercial applications. The sheet is heated to a softened state and subsequently deformed in a mold using applied pressure, a vacuum, a moving plug, or a combination of these. The thermoforming market is expanding to include more complex geometries and a wider range of potential materials. Material must be selected early in the product development process, based on cost, service properties, and processability.

However, in the thermoplastic forming industry, it is a common practice to mostly rely on trial and error methods based on a high number of test specimens in order to assess the actual mass production planning and schedule, a procedure that involves costly operations. This situation also occurs when designing a new product or while improving existing processes. It is therefore appealing to develop more efficient alternatives based for example on reliable numerical predictive tool for the analysis and optimisation of these manufacturing processes. This is enabled by the fact that it is now possible to develop precise sophisticated models describing not only the thermal and mechanical phenomena taking place within the materials but also describing the interactions between the different components of the fabrication system. These mathematical models are then implemented into user friendly computer softwares that are validated through laboratory tests before their actual implementation in industrial product design and system manufacturing simulation.

In the finite element codes used to handle these problems, the application of loadings is in general defined in terms of pressure. For such kind of loading, quasi-static problems are largely discussed in the technical literature, among which one can mention the following works (DeLorenzi & Nied, 1991), (Laroche & Erchiqui, 2000) for hyperelastic materials and (Laroche & Erchiqui, 1998) for viscoelastic materials. For the case of dynamic problems, actually less considered than their quasi-static counterparts, we can mention references like (Verron & al, 2001), (Erchiqui & al, 2001) for thermoplastic materials. In these problems, strong mechanical and geometric non linearities induce instabilities during blowing and

thus require, for quasi-static problems, an accurate control of the loadings employed in the simulation (Khayat & al, 1992) and for dynamic problems, an adequate time step control (Lapidus & Pinder, 1982). These instabilities, associated with the descending segment of the load-deformation curve, correspond physically to regions in which the load (pressure) decreases while the expansion is still going on. In order to be able to follow the loading curve, we consider the dynamic problem of thermoforming of the viscoelastic and the hyperelastic sheet subjected to air flow loading (Erchiqui & al, 2005). The Inflation process of the membrane is controlled by the gas equation of state. The dynamic pressure is thus deduced from one of the three equations of state: the Redlich–Kwong, the van der Waals and the ideal equations.
For modeling purposes, we adopt the finite element method based on the Lagrangian formulation. Membrane theory and material incompressibility assumptions are considered. The membrane structure is discretized by plane finite elements (Zienkiewicz & Taylor, 1991) and time integration is performed via an explicit algorithm based on central difference method that is conditionally stable (Lapidus & Pinder, 1982). For constitutive behavior, the viscoelastic integral models of Lodge (Lodge, 1964) and Christensen (Christensen, 1980) type and the hyperelastic models of Mooney-Rivlin (Rivlin, 1948) and Ogden (Ogden, 1972) type are considered. Moreover, the influence of all these material constitutive models on the thickness distribution for thermoforming a part in ABS is analysed using a dynamic loading by air flow characteristics.

2. Kinematics

We consider a viscoelastic material medium, occupying a deformable continuous body $\mathbf{\Omega}$ of surface $\mathbf{\Gamma}$. Each material point P, belonging to the body $\mathbf{\Omega}$, can be identified by using three curvilinear co-ordinates $\left(\theta^1,\theta^2,\theta^3\right)$, which remain constant at the time of inflation. In the case of a thin viscoelastic structure, the number of these curvilinear co-ordinates can be reduced to two $\left(\theta^1,\theta^2\right)$ defined on the membrane's mid surface. Consequently, the position of a point P belonging to this mid surface will be defined, in the undeformed reference configuration, by the vector $\mathbf{X}\left(\theta^1,\theta^2\right)$, and, in the deformed configuration, by the vector $\mathbf{x}\left(\theta^1,\theta^2\right)$. Also, at the mid surface point P, we associate, in the reference configuration, a thickness function $\mathbf{H_0}\left(\theta^1,\theta^2\right)$ and local tangent vectors $\left(\mathbf{G_1},\mathbf{G_2}\right)$, and in the deformed configuration, we associate a thickness $\mathbf{h}\left(\theta^1,\theta^2\right)$ and local tangent vectors $\left(\mathbf{g_1},\mathbf{g_2}\right)$. Thus, given the structure mid surface parameterizations defined by, $\mathbf{X}\left(\theta^1,\theta^2\right)$ and $\mathbf{x}\left(\theta^1,\theta^2\right)$, the introduced tangent vectors can be determined from the following classical formula:

$$\mathbf{G_1}=\frac{\partial \mathbf{X}}{\partial \theta^1},\ \mathbf{G_2}=\frac{\partial \mathbf{X}}{\partial \theta^2} \tag{1}$$

$$\mathbf{g_1}=\frac{\partial \mathbf{x}}{\partial \theta^1},\ \mathbf{g_2}=\frac{\partial \mathbf{x}}{\partial \theta^2} \tag{2}$$

However, in order to describe the deformation in the direction perpendicular to the thin structure's mid surface, the information on the tangent vectors $(\mathbf{G_1},\mathbf{G_2})$ and $(\mathbf{g_1},\mathbf{g_2})$ must be supplemented by out-of-plane information. To address this situation, we introduce two unit vectors, $\mathbf{G_3}$ and $\mathbf{g_3}$, orthogonal to the surface covariant base vectors $(\mathbf{G_1},\mathbf{G_2})$ and $(\mathbf{g_1},\mathbf{g_2})$ defined respectively by:

$$\mathbf{G}_3 = \mathbf{N} = \frac{\mathbf{G}_1 \times \mathbf{G}_2}{\|\mathbf{G}_1 \times \mathbf{G}_2\|},\ \mathbf{g}_3 = \mathbf{n} = \frac{\mathbf{g}_1 \times \mathbf{g}_2}{\|\mathbf{g}_1 \times \mathbf{g}_2\|} \tag{3}$$

Vectors **N** and **n** are outward unit vectors normal to the tangent planes defined by vectors $(\mathbf{G_1},\mathbf{G_2})$ and $(\mathbf{g_1},\mathbf{g_2})$, respectively. The displacement field generated by the movement of point **P** of the membrane's mid surface can be described by a function **u** defined by (difference between the current position vector and the reference undeformed position vector):

$$\mathbf{u} = \mathbf{x} - \mathbf{X} \tag{4}$$

As a measure of the deformation of the membrane, we use the generalized Green-Lagrangian strain, whose components are:

$$\underline{\underline{\mathbf{E}}}_{\alpha\beta} = \frac{1}{2}\left(\mathbf{g}_\alpha^{\mathbf{T}} \cdot \mathbf{g}_\beta - \mathbf{G}_\alpha^{\mathbf{T}} \cdot \mathbf{G}_\beta\right),\ \alpha,\beta = 1,2 \tag{5}$$

The notation $*^{\mathbf{T}}$ denotes the transposition of the line vector associated with the column vector $*$. To describe the deformed covariant basis vector, $\mathbf{g}_\alpha$, in terms of covariant undeformed basis vector $\mathbf{G}_\alpha$, we use the transformation:

$$\mathbf{g}_\alpha = \underline{\underline{\mathbf{F}}} \cdot \mathbf{G}_\alpha \tag{6}$$

where $\underline{\underline{\mathbf{F}}}$ is the deformation gradient tensor at **x :**

$$\underline{\underline{\mathbf{F}}} = \underline{\underline{\mathbf{I}}} + \nabla\mathbf{u} \tag{7}$$

$\underline{\underline{\mathbf{I}}}$ is the second-order identity tensor. Thus, relative to the reference configuration, the Green-Lagrange deformation tensor, given in general curvilinear co-ordinates by (5), becomes, in matrix form:

$$\underline{\underline{\mathbf{E}}} = \frac{1}{2}\left(\underline{\underline{\mathbf{C}}} - \underline{\underline{\mathbf{I}}}\right) \tag{8}$$

where $\underline{\underline{\mathbf{C}}}$ is the right Cauchy-Green deformation tensor defined by $\underline{\underline{\mathbf{C}}} = \underline{\underline{\mathbf{F}}}^{\mathbf{T}} \cdot \underline{\underline{\mathbf{F}}}$. The virtual Green-Lagrange deformation tensor then becomes:

$$\delta\underline{\underline{\mathbf{E}}} = \frac{1}{2}\left(\delta\underline{\underline{\mathbf{F}}}^{\mathbf{T}} \cdot \underline{\underline{\mathbf{F}}} + \underline{\underline{\mathbf{F}}}^{\mathbf{T}} \cdot \delta\underline{\underline{\mathbf{F}}}\right) \tag{9}$$

3. Preliminary considerations

The problem of thin structure material inflation can be modelled by considering the large deformation of the body with finite strain. The continuum formulation using the updated Lagrangian description is presented using a 3-node isoparametric element. Although the

formulation is applicable for the 3D geometry, the finite element discretization is shown for the plane strain configuration only, for the sake of simplicity. The discussion is followed by a membrane formulation, and the solution method.

4. Dynamic force balance equation

We utilize the dynamic finite element method with both space and time discretization to simulate the inflation of the thermoplastic membrane. Thus, the principle of virtual work is expressed on the undeformed configuration for the inertial effects and internal work. Then, this weak form of the principle of virtual work is discretized and assembled by applying the finite elements methodology (Erchiqui & al, 2005). Because of the presence of the inertial force, a time discretization is required. This is handled here through the introduction of a centred finite difference technique that is conditionally stable (Lapidus & Pinder, 1982).

4.1 Virtual work expression

In the reference configuration, the expression of the principle of virtual work is given by the following formula (Erchiqui & al, 2005):

$$\delta W = \int_{\Omega_0} \delta E : S \, d\Omega_0 + \int_{\Omega_0} \rho_0 \ddot{u}^T \cdot \delta u \, d\Omega_0 + \int_{\Omega_0} f_0 \cdot \delta u \, d\Omega_0 - \int_{\Gamma} \delta u^T \cdot t \, d\Gamma \tag{10}$$

where $\underline{\underline{\mathbf{S}}}$ is the second Piola-Kirchhoff stress tensor, $\boldsymbol{\Gamma}$ is the surface of the deformed membrane, $\underline{\mathbf{t}}$ is the external surface force due to pressure and $\boldsymbol{\delta u}$ is a virtual displacement vector compatible with the displacement boundary conditions. The principle of virtual work expression, given by Eqn. (10), can be broken up into four terms:

$$\delta W(u, \delta u, t) = \delta W^{int} + \delta W^{acc} + \delta W^{grav} - \delta W^{ext} \tag{11}$$

where $\boldsymbol{\delta W^{int}}$, $\boldsymbol{\delta W^{acc}}$, $\boldsymbol{\delta W^{ext}}$ and $\boldsymbol{\delta W^{grav}}$ are the internal, inertial external and body work, respectively:

$$\delta W^{int} = \int_{\Omega_0} \delta E : S \, d\Omega_0 \tag{12.a}$$

$$\delta W^{ext} = \int_{\Gamma} \delta u^T \cdot t \, d\Gamma \tag{12.b}$$

$$\delta W^{acc} = \int_{\Omega_0} \rho_0 \ddot{u}^T \cdot \delta u \, d\Omega_0 \tag{12.c}$$

$$\delta W^{grav} = \int_{\Omega_0} f_0 \cdot \delta u \, d\Omega_0 \tag{12.d}$$

By introducing the pressure force, $\underline{\mathbf{t}} = \Delta p(t).\mathbf{n}$, which depends on the deformed geometry, we obtain for the external work:

$$\delta W^{ext.} = \int_{\Gamma} \Delta p \delta u^T \cdot n \, d\Gamma \qquad \forall \delta u \tag{12.e}$$

where $\Delta \mathbf{p}$ represents the internal pressure.

4.2 Spatial approximation

After summation of all element contributions, the inflation problem is then reduced to the following discrete system of equations:

$$\mathbf{F_{acc}} + \mathbf{F_{grav}} + \mathbf{F_{int}} - \mathbf{F_{ext}} = 0 \tag{13}$$

where $\mathbf{F_{acc}}$, $\mathbf{F_{ext}}$, $\mathbf{F_{grav}}$ and $\mathbf{F_{int}}$ are the global nodal inertial, external, body and internal force vectors experienced by the thermoplastic membrane. By introducing the mass matrix **M** associated with the inertial forces, the inflation problem can then be reduced to a system of second-order ordinary differential equations:

$$\mathbf{M} \cdot \ddot{\mathbf{u}}(\mathbf{t}) = \mathbf{F_{ext}} + \mathbf{F_{grav}} - \mathbf{F_{int}} \tag{14}$$

The system (14) is decoupled by applying the diagonalization method of (Lapidus & Pinder, 1982) to matrix **M,** which transforms it into a diagonal mass matrix, $\mathbf{M^d}$.

4.3 Time discretization

Knowing the velocity and acceleration vectors at time t_n, it is possible, by using a time integration scheme, to calculate the displacement vector at a discrete time t_{n+1}. A centered finite difference scheme is adopted here (Erchiqui & al, 2005), and Eqn. (14) then becomes:

$$\mathbf{u_i}(\mathbf{t}+\Delta\mathbf{t}) = \frac{\Delta\mathbf{t}^2}{\mathbf{M_{ii}^d}}\left(\mathbf{F_i^{ext.}}(\mathbf{t}) + \mathbf{F_i^{grav.}}(\mathbf{t}) - \mathbf{F_i^{int.}}(\mathbf{t})\right) + 2\mathbf{u_i}(\mathbf{t}) - \mathbf{u_i}(\mathbf{t}-\Delta\mathbf{t}) \tag{15}$$

$\mathbf{M_{ii}^d}$ are the diagonal components of the matrix $\mathbf{M^d}$.

4.4 Stability limit of the dynamic explicit method

Advancing a time step of this scheme requires a lot of calculations. The price paid for this simplicity is *conditional stability* (Lapidus & Pinder, 1982). If the dynamic system includes phenomena which evolve more rapidly than the approximate solution itself, these will be incorrect for exponentially increasing components of the solution. This *instability* typically results in the blow-up of the solution. Conditional stability for mechanical problems is expressed through the Courant-Friedrichs-Lewy criterion: the time step must be smaller than the critical time steps $\Delta\mathbf{t_{crit}}$:

$$\Delta t \le \Delta t_{crt} = \varepsilon \frac{d}{c} \tag{16}$$

Here **c** is the wave speed in the medium and ***d*** the element size. The quantity ***d/c*** is the time that a wave needs to propagate across an element of size ***d***. The proportionality constant, ε, depends on the integration scheme used.

5. Gas equations of state and pressure loading

In addition to the traditional approach, which considers loads in pressures for the numerical modeling of the free and confined inflation in the viscoelastic structures, there is a relatively recent approach which considers gas flows for modeling (Erchiqui, 2007). This is correct at normal temperatures and pressures. At low temperatures or high pressures, real gases deviate significantly from ideal gas behavior. Indeed, at normal pressures, the volume

occupied by the atoms or molecules is a negligibly small fraction of the total volume of the gas. But at high pressures, this is no longer true. As a result, real gases are not as compressible under high pressures as an ideal gas. The volume of a real gas is larger than the expected one from the ideal gas equation at high pressures. Moreover, the assumption of the absence of a force of attraction between ideal gas particles involves a violation of the physical observations such as these gases cannot condense to form liquids. In reality, there is a small force of attraction between gas molecules, which tends to hold them together. This force of attraction has two consequences: (1) gases condense to form liquids at low temperatures; and (2) the pressure of a real gas is sometimes smaller than expected for an ideal gas. To be in conformity with these observations, we are interested in this work by the laws of state which characterize real gases such as: the van de Waals gas and Redlich-Kwong state equations, in addition to the equation of ideal gases. Theses equations will enable determination of the acceptable dynamic pressure field distribution during free and confined inflation.

The assumptions used for the calculation of the dynamic pressure are:

i) Gas temperature is assumed constant (T_{gas});
ii) Pressure between the sheet and mould is assumed to be constant (p_0).

If we represent by V_0 an initial volume enclosing the membrane at the initial time t_0 and containing a number n_0 of gas moles (we assume that the forming process temperature is constant), then, for the cases of the ideal, Van Der Waals and the Redlich-Kwong equations of states of gas:

a) Ideal gas equation

The ideal gas equation of state is given by:

$$P_0 = \frac{n_0 R T_{gas}}{V_0} \tag{17}$$

P_0 is the initial pressure and R is the universal gas constant

b) Van der Waals gas equation

The van der Waals equation of state is given by (Landau & Lifshitz, 1984):

$$P_0 = \frac{n_0 R T_{gas}}{V_0 - n_0 b} - \frac{n_0^2 a}{V_0^2} \tag{18}$$

Parameters *a* and *b* are constants that change from gas to gas. The constant b is intended to account for the finite volume occupied by the molecules, the term an_0^2/V_0^2 account for the initial forces of attraction between molecules. Please note that when a and b are set at zero, the ideal gas equation of state results.

c) *Redlich-Kwong gas equation*

The Redlich-Kwong equation of state is given by (Redlich & Kwong, 1949):

$$P_0 = \frac{n_0 R T_{gas}}{V_0 - n_0 b} - \frac{n_0^2 a}{V_0 (V_0 + n_0 b)\sqrt{T_{gas}}} \tag{19}$$

where parameters a and b are calculated in terms of the values of pressure p_c and temperature T_c at the critical point of the gas under examination, i.e.:

$$a = 0.42748 \frac{\overline{R}^2 T_c^{2.5}}{p_c} \text{ and } b = 0.08664 \frac{\overline{R} T_c}{p_c} \tag{20}$$

With $\overline{R} = 8.314 kJ / kmol.K$.

Now if we represent by n(t) the additional number of moles of gas introduced for the inflation of the thermoplastic membrane, by p(t) the internal pressure and by V(t) the additional volume occupied by the membrane at time t, we get the following relations:

a) Ideal gas equation

$$\Delta P = P(t) - P_0 = \left[\frac{(n(t) + n_0) R T_{gas}}{(V(t) + V_0) - (n(t) + n_0) b} \right] - \left[\frac{n_0 R T_{gas}}{V_0 - n_0 b} \right] \tag{21}$$

b) Van der Waals gas equation

$$\Delta P = P(t) - P_0 = \left[\frac{(n(t) + n_0) R T_{gas}}{(V(t) + V_0) - (n(t) + n_0) b} - \frac{(n_0 + n(t))^2 a}{(V(t) + V_0)^2} \right] - \left[\frac{n_0 R T_{gas}}{V_0 - n_0 b} - \frac{n_0^2 a}{V_0^2} \right] \tag{22}$$

c) Redlich-Kwong gas equation

$$\Delta P(t) = P(t) - P_0 = \left[\frac{(n(t) + n_0) R T_{gas}}{(V(t) + V_0) - (n(t) + n_0) b} - \frac{(n(t) + n_0)^2 a}{(V(t) + V_0)\left((V(t) + V_0) + (n(t) + n_0) b\right)\sqrt{T_{gas}}} \right] - \left[\frac{n_0 R T_{gas}}{V_0 - n_0 b} - \frac{n_0^2 a}{V_0 (V_0 + n_0 b)\sqrt{T_{gas}}} \right] \tag{23}$$

Each equation, 21-23, represents the time evolution of pressure inside the thermoplastic membrane, closely related to the evolution of the internal volume of the membrane via the thermodynamic state equation. In these cases, the external virtual work becomes:

a) ideal gas equation

$$\delta \mathbf{W}^{\mathbf{ext.}} = \int_{\Gamma} \left(\left[\frac{\left(n(t)+n_0\right) RT_{gas}}{\left(V(t)+V_0\right)} \right] - \left[\frac{n_0 RT_{gas}}{V_0} \right] \right) \delta \mathbf{u}^{\mathbf{T}} \cdot \mathbf{n} \ \ \mathbf{d\Gamma} \ \ \forall \ \ \delta \mathbf{u} \tag{24}$$

b) Van der Waals gas equation

$$\delta \mathbf{W}^{\mathbf{ext.}} = \int_{\Gamma} \left(\left[\frac{\left(n(t)+n_0\right) RT_{gas}}{\left(V(t)+V_0\right) - \left(n(t)+n_0\right) b} - \frac{\left(n_0 + n(t)\right)^2 a}{\left(V(t)+V_0\right)^2} \right] - \left[\frac{n_0 RT_{gas}}{V_0 - n_0 b} - \frac{n_0^2 a}{V_0^2} \right] \right) \delta \mathbf{u}^{\mathbf{T}} \cdot \mathbf{n} \ \ \mathbf{d\Gamma} \ \ \forall \ \ \delta \mathbf{u} \tag{25}$$

c) Redlich-Kwong gas equation

$$\delta \mathbf{W}^{\mathbf{ext.}} = \int_{\Gamma} \left[\begin{array}{l} \left[\dfrac{\left(n(t)+n_0\right) RT_{gas}}{\left(V(t)+V_0\right) - \left(n(t)+n_0\right) b} - \dfrac{\left(n(t)+n_0\right)^2 a}{\left(V(t)+V_0\right)\left(\left(V(t)+V_0\right) + \left(n(t)+n_0\right) b\right)\sqrt{T_{gas}}} \right] \\ \quad - \left[\dfrac{n_0 RT_{gas}}{V_0 - n_0 b} - \dfrac{n_0^2 a}{V_0 \left(V_0 + n_0 b\right)\sqrt{T_{gas}}} \right] \end{array} \right] \delta \mathbf{u}^{\mathbf{T}} \cdot \mathbf{n} \ \ \mathbf{d\Gamma} \ \ \forall \ \ \delta \tag{26}$$

The advantage of using a load expressed in term of gas flow instead of pressure loading is that it allows natural exploration of the load-deformation curve and nor worry about the instability phenomenon encountered when classical pressure loading is employed. The introduction of constant pressure as a loading force instead of gas flow velocity in the two used finite element formulations, quasi-static and dynamic, leads to a divergence of the computations for the values of pressure beyond the critical point (starting of the unstable segment of the load-deformation curve) (Erchiqui & al, 2001).

6. Implemented constitutive models

In this work, we consider the assumptions of the plane stresses and of the incompressibility of the thermoplastic material. It follows that the components of the Cauchy stress tensor have the following properties:

$$\sigma_{13} = \sigma_{23} = \sigma_{31} = \sigma_{32} = \sigma_{33} = 0 \tag{27}$$

In the thermoforming of cut sheet, the polymer is subsequently heated in an oven and thermoformed, usually under vacuum. The sheet forming operation is characterized by rapid deformation of the sheet. Modeling of this stage of the process can be done by using either hyperelastic or viscoelastic constitutive equation since the time dependence of the deformation in not critical.

Hyperelastic materials are defined by the existence of scalar function $W(\mathbf{F})$ called the strain energy function, from which stresses can be derived at each point. In order to satisfy the objectivity requirements, the strain energy function must be invariant under changes of the observer frame of reference. It is well known that the Cauchy-Green deformation tensor is invariant under changes of the observer frame of reference. Thus, if the strain energy function can be written as a function of **C**, it automatically satisfies the objective principle.

The general stress-strain relationship is given by the formula:

$$S_{ij} = 2\frac{\partial W}{\partial C_{ij}} \tag{28}$$

where **S** is the Piola-Kirchhoff stress tensor.
The different models that exist in the literature define the strain energy as a function of the strain field. The Rivlin theory (Rivlin, 1948) for isotropic materials describes the energy as a function of the three Cauchy strain invariants I_1, I_2 and I_3. Assuming the incompressibility of the material, the stress can be obtained from the following Mooney-Rivlin form:

$$W = \sum_{i+j=1}^{N} (I_1 - 3)^i (I_2 - 3)^j \tag{29}$$

The use of two terms in the series is sufficient to describe the elastic modulus in both uniaxial and biaxial deformation modes.
Another popular strain energy formulation is the Ogden model (Ogden, 1972) that uses the principal values λ_i (*i=1, 2, 3)* from the right Green-Cauchy strain tensor:

$$W = \sum_{i=1}^{N} \frac{\alpha_i}{\mu_i} \left(\lambda_1^{\mu_i} + \lambda_2^{\mu_i} + \lambda_3^{\mu_i} - 3 \right) \tag{30}$$

where α_i and μ_i are the material constants. The use of two terms in the series is usually sufficient to describe the material no-linear response under deformation.
Integral type viscoelastic models relate the true stress to the strain history. These models are more appropriate for representing polymers at the liquid (Lodge, 1964) or semi-solid state (Christensen, 1980), (Laroche & Erchiqui, 2000). In this work, to analyze the viscoelastic behavior and isotropic thermoplastic materials, we consider the Lodge model and Christensen model.
The Lodge model (Lodge, 1964) has been developed for representing the viscoelastic deformation of liquid materials. For this model, the Cauchy stress tensor σ, is related at time t to the history of the Finger deformation tensor **B** by:

$$\sigma(t) = -p(t)\, I + \int_{-\infty}^{t} \sum_{k} \frac{g_k}{\tau_k} e^{-(t-\tau)/\tau_k} B(\tau, t)\, d\tau \tag{31}$$

where the Finger tensor **B** is related to the right Cauchy Green deformation tensor **C** by:

$$B = C^{-1} = \left[F^T F \right]^{-1} \tag{32}$$

F is the deformation gradient tensor, **I** is the identity tensor, *p* is the hydrostatic pressure, g_k and τ_k representing respectively the relaxation modulus and the relaxation time. The hydrostatic pressure *p* result from the plane stress state due to membrane hypothesis $\sigma_{zz}=0$.
The Christensen model (Christensen, 1980), has been developed for representing the viscoelastic deformation of solids. It can be used for the thermoforming of semi-solid materials. This model gives the second Piola-Kirchhoff stress tensor **S** at time *t* as a function of the Lagrangian strain history **E**:

$$S(t) = -p(t)\, C^{-1} + g_0\, I + \int_{-\infty}^{t} g_1(t-\tau) \frac{\partial E(\tau, t)}{\partial \tau}\, d\tau \tag{33}$$

where g_0 is the hyperelastic modulus and g_1 is the material relaxation function given by equation:

$$g_l = \sum_k C_k e^{-(t-\tau)/\tau_k} \tag{34}$$

where C_k is the stiffness modulus. In a Lagrangian formulation, we consider, for our numerical modeling, the second Piola-Kirchhoff stress tensor **S** defined by the following transformation:

$$S(t) = J(t)\, F^{-1}(t)\, \sigma(t)\, F^{-T}(t) \tag{35}$$

where the **J(t)** is the Jacobian of the transformation. In the case of incompressible thermoplastic materials, the jacobian is unity:

$$J(t) = \det(F) = 1 \tag{36}$$

In our study, for the plane stress state, the deformation and stress matrices, **C**(t) and **S**(t), have respectively the following forms:

$$[C(t)] = \begin{bmatrix} C_{xx}(t) & C_{xy}(t) & 0 \\ C_{xy}(t) & C_{yy}(t) & 0 \\ 0 & 0 & C_{zz}(t) \end{bmatrix} \tag{37}$$

$$[S(t)] = \begin{bmatrix} S_{xx}(t) & S_{xy}(t) & 0 \\ S_{xy}(t) & S_{yy}(t) & 0 \\ 0 & 0 & 0 \end{bmatrix} \tag{38}$$

The term $C_{zz}(t)$ in equation (37) can be directly computed from the other components of the deformation tensor:

$$C_{zz}(t) = \lambda_3^2(t) = \frac{1}{C_{xx}(t)C_{yy}(t) - C_{xy}(t)C_{xy}(t)} \tag{39}$$

Where $\lambda_3(t)$ is the principal stretch ratio in thickness direction defined by:

$$\lambda_3(t) = \frac{h(t)}{h_0} \tag{40}$$

where $h(t)$ and h_0 are membrane thicknesses respectively in the deformed and undeformed configurations.

The memory integral constitutive equation can be easily extended to incorporate temperature changes which may occur during the thermoforming history.

The adopted strategy for the computer implementation of the finite element formulation, developed above for the computation of the nodal displacements $\vec{u}_{n+1}$ at time t_{n+1}, see the reference (Erchiqui & al, 2001).

7. Numerical validation: equation of state effect in free inflation of membrane

The dynamic finite element method outlined in the previous section was implemented in the general purpose finite element code ThermoForm, developed by the author. This code was developed in order to study the stresses and deformation arising in thermoforming sheet and stretch-blow molding problems. All computations were performed on a PC in single precision.

For numerical modeling, we considered for the outside pressure forces, induced by the airflow used for blowing the membrane, the three expressions associated respectively of the ideal gas equation of state (17), the van der Waals equation of state (18) and Redlich-Kwong equation of state (19). The rheological parameters used for the Lodge law of behaviour are found in Table 1, for HDPE-6200 material.

Lodge Model Constants at Reference Temperature	
g_k (MPa)	τ_k (second)
0.21177	0.007140
0.07837	0.049970
0.03165	0.349854
0.01122	2.448980
0.00324	17.14286
0.00117	120.0000
WLF parameters	
T_{ref} (^{0}C)	150.0
C_1	2.915
C_2 (^{0}C)	50.00

Table 1. Viscoelastic material constants for HDPE-6200

As a first application, we consider the free inflation of a square membrane (length = 15.0cm) made of HDPE material; with a load in terms of a non-linear air flow rate, similar to what is found in the practical applications (see Fig.1). The material temperature is supposed to be constant and equal to 140^{o}C. Blowing time is fixed at 1.0s. The sheet is discretized by triangular membrane elements and its sides are fixed. The numerical analysis has been performed in two cases: i) initial sheet thickness, h_0, was 1.50 mm and ii) initial sheet thickness was 3.00 mm.

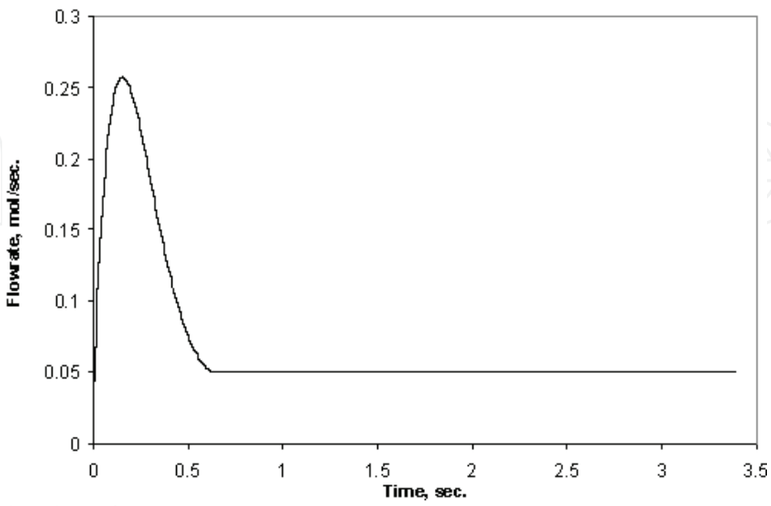

Fig. 1. Air flow loading function

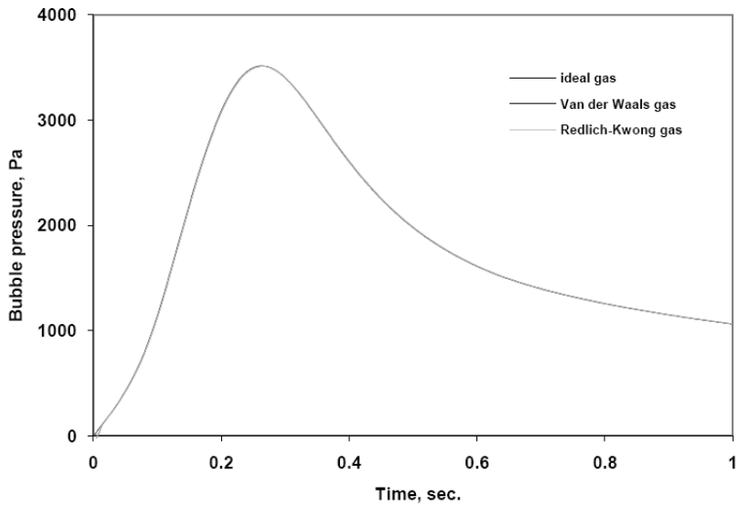

Fig. 2. Bubble pressure *vs* times, h_0=1.5 mm

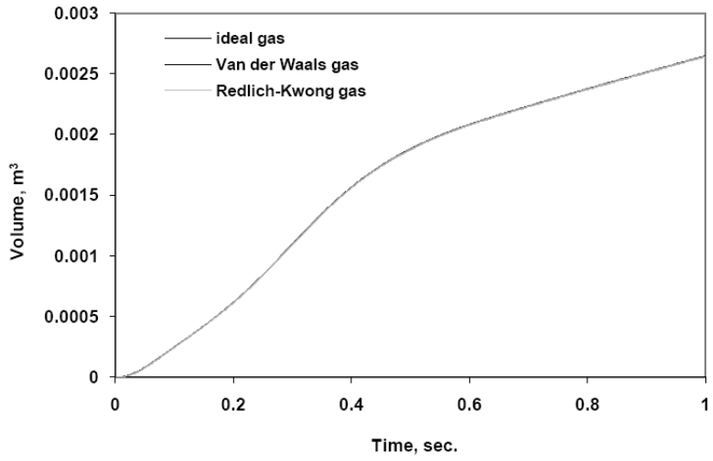

Fig. 3. Bubble volume *vs* times, h0=1.5 mm

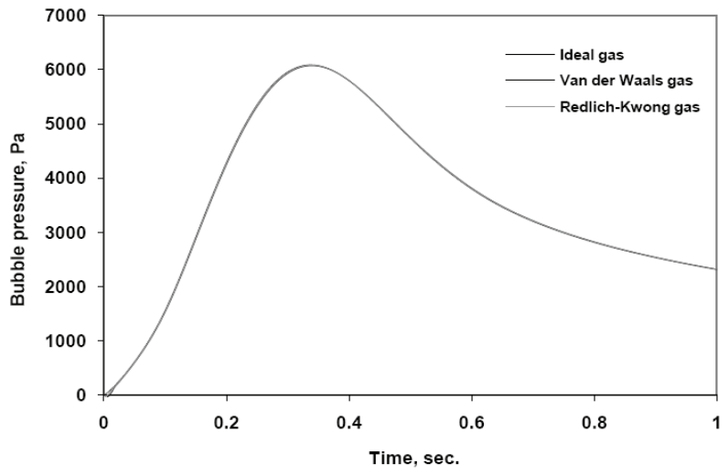

Fig. 4. Bubble pressure *vs* times, h_0=3.0 mm

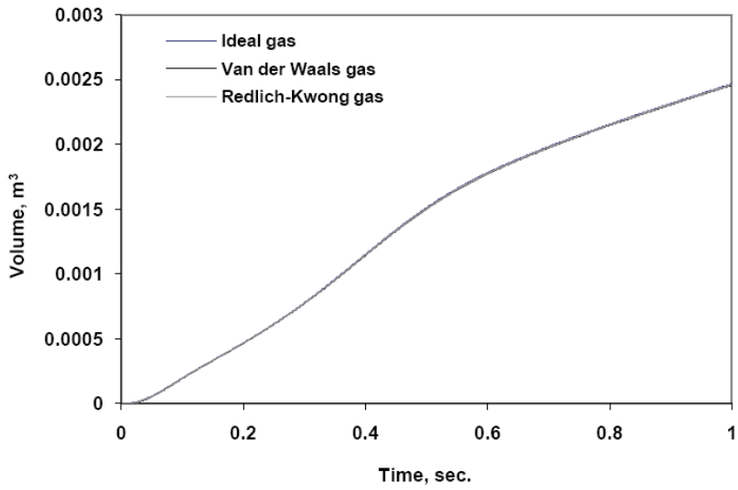

Fig. 5. Bubble volume *vs* times, h_0=3.0 mm

Figures 2-3 illustrate, respectively, the evolution of the internal thermoplastic pressure and volume *vs* time, obtained by the Thermoform finite element code, in the first case (h_0 = 1.50 mm). We notice that the three equations of states predict similar results. The absolute relative average error between the ideal gas equation of state and the two other models is lower than 0.15%. Even remarks in the second case where h_0 = 3mm (see Figures 4-5).

8. Characterization

Deformation of a flat polymer sheet clamped around its edges into a 3D shape is the main feature of the thermoforming process. Generally the deformation is of a non-uniform multi-axial type and takes place at a forming temperature above the glass transition temperature. In this work, the bubble inflation technique (Joye & *al*, 1972) is used for the purpose of fitting the constitutive models used in the numerical simulation of the thermoforming process. The experimental set up has been described elsewhere (Derdouri & *al*, 2000).

The determination of hyperelastic and viscoelastic constants is performed with a biaxial characterization technique (Joye & *al*, 1972). This technique consists in a controlled free inflation of a sheet where the air flow rate is controlled while the forming pressure and sheet height are measured. The sheet is considered thin enough to be modeled by the following axisymmetric membrane inflation relationship:

$$\frac{d\vec{u}(R)}{dR} = \vec{F}(\vec{u}(R), R) \tag{41}$$

and

$$\vec{u}(R) = \{\lambda_1(R), \lambda_2(R), \theta(R), z(R), P(R)\} \tag{42}$$

where λ_1 and λ_2 are the two stretch ratios in meridian and circumferential directions respectively. θ, R and z represent the angular, circumferential and vertical position respectively. The internal pressure is given by P_e and is considered uniform on the membrane surface.

Theoretical material constants are obtained by minimizing the global absolute error, E, between the computed pressure, P_c, and the measured pressure, P_e, at each time step:

$$E = \sum_{i=1}^{N_{exp}} [P_c(t_i) - P_e(t_i)]^2 \tag{43}$$

where N_{exp} represent the number of experimental points represents. The problem of minimization of the error is solved by an algorithm of Levenberg-Marquardt (Marquardt, 1963), (Levenberg, 1944). The system descripting the balance of the blowing membrane is solved by the finite differences method with differed corrections (Dennis & Schabel, 1983).

8.1 Numerical validation

As a validation of the formulation described above, we consider the problem of free blowing of a viscoelastic membrane. The material considered in this stage of work is acrylonitrile-butadiene-styrene (ABS). The initial sheet thickness was 1.57 mm. The exposed circular domain of radius R_0=3.175 cm is heated to the softening point inside a heating chamber using infrared heaters. When the temperature was quite uniform over the flat sheet, the inflation was started using compressed air at a controlled flow rate. In most inflation tests the experiment ended when the bubble burst. The bubble pressure, its height at the pole and time are recorded simultaneously using a video camera and a data acquisition system.

The measured pressure was interpolated by a polynomial function (Erchiqui & al, 2001) and used in the finite element program to compute the time evolution of the bubble height at the pole. The predictions obtained with Ogden Mooney-Rivlin and Lodge models give almost identical results and are shown against experimental data in Figure 6, at a setting temperature of 143°C. We notice that the the Mooney-Rivlin model, the Ogden model and the Lodge model all predict similar bubble height at the pole, which is close to the experimental measurements. However, the three models give different results, however close to the experimental measurements, when the bubble pressure level is close to the maximum pressure reached during experiments (Erchiqui & al, 2001).

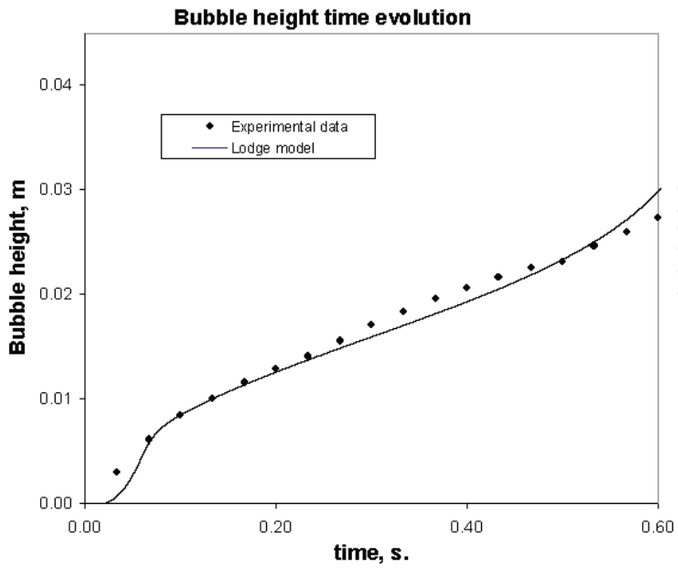

Fig. 6. Bubble height time evolution

8.2 Thermoforming application

Like the circular viscoelastic membrane blowing application of the previous section, we also use in this section, the dynamic approach with a load applied in term of linear air flow rate, to study the thermoforming of a container made of ABS material. The geometries of the mold and the parison, with a grid using the triangular elements membranes (936 nodes and 1756 elements), are presented on figure 7. The initial membrane configuration is a rectangular sheet with a length of 25.4 cm, a width of 15.24 cm and a uniform thickness of 0.16 cm and its edges are considered as fixed. In this example, only the influence of the Lodge and the Christensen constitutive models on the thickness, in the thermoforming sheet, is analyzed. However, in the paper, we present a comparative analysis on the thickness and the stress distribution in the thermoforming sheet for the viscoelastic behavior (Lodge, Christensen) and hyperelastic (Mooney-Rivlin, Ogden). The rheological parameters used for these materials can be found in (Erchiqui & *al*, 2001).

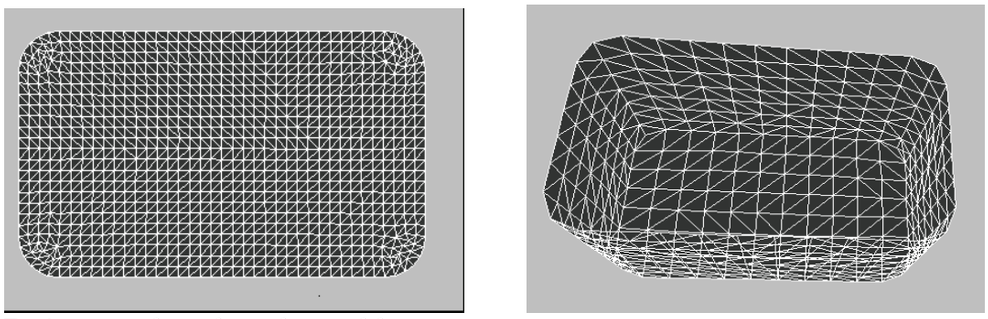

Fig. 7. Parison mesh and mesh mould

These parameters were obtained using the biaxial technique of material parameter identification (Derdouri & al, 2000), for a working temperature of 143°C. For the contact of the preform and the mold, we considered the assumption of sticking contact, because it is estimated that the polymer cools and stiffens quickly (at the time of the contact between the thermoplastic parison, which is very hot, and molds it, which is cold) and that the pressure of working is not sufficient to deform the part of the membrane which is in contact with mold (DeLorenzi & Nied, 1991). The time of blowing (time necessary so that the last node of the parison returns in contact with the mold), for the air flow used by our simulation, according to our numerical calculations, is about 1 second for the Lodge material, 1.15 second for the Christensen material, 0.76 second for the Ogden material and 0.72 second for the Mooney-Rivlin material.

In figure 8-9, we presented, for the models (Lodge, Christensen, Ogden Mooney Rivlin) the final thickness distribution $h=h_0\backslash\lambda_3$ (h_0 is the thickness in the undeformed configuration) on the half-planes of symmetry XZ and YZ in the thermoformed container.

A comparison study of the numerical results obtained, for the thermoforming of the ABS thermoplastic part, shows that there is a small difference in the results predicted by our modeling calculations for the four behavioral constitutive models. Indeed, the ABS thermoplastic membrane was characterized for the viscoelastic models of Lodge, Christensen, Mooney-Rivlin and Ogden. It thus follows, that theoretically the use of the rheological parameters obtained by biaxial identification (Erchiqui & al, 2001), in modeling, must, a priori, lead to the same final thickness distribution on the half-planes XZ and YZ of symmetry.

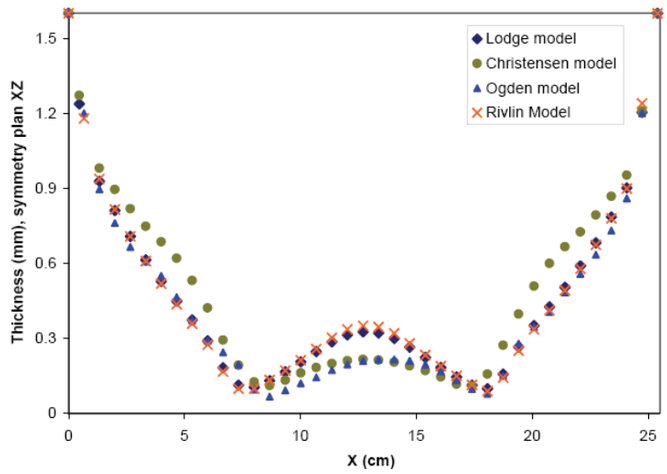

Fig. 8. Thickness distribution, symmetry plan XZ

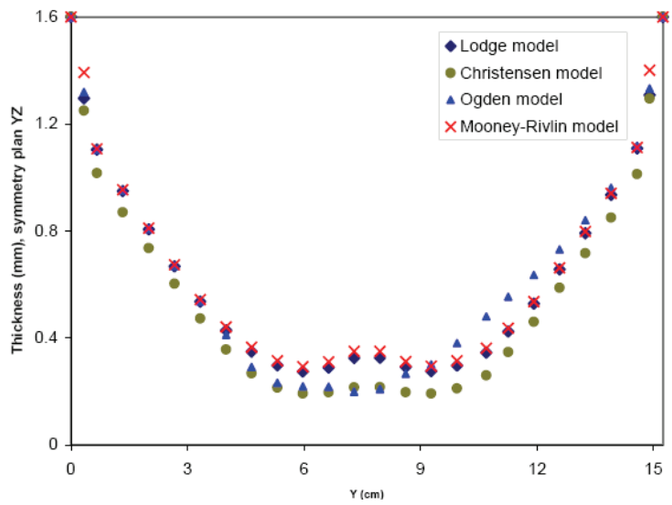

Fig. 9. Thickness distribution, symmetry plan YZ

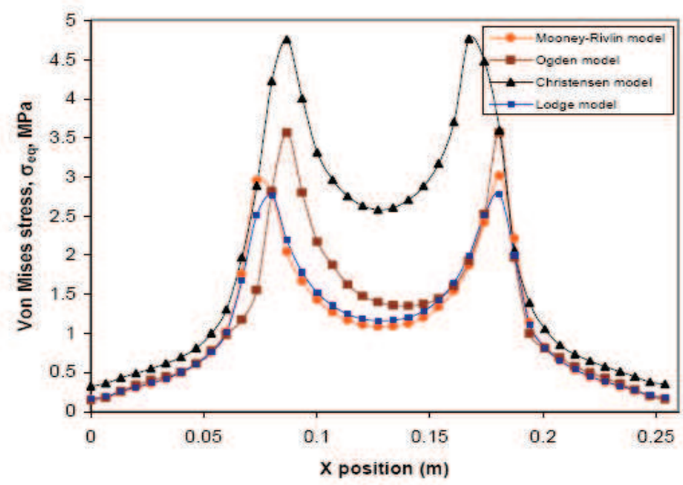

Fig. 10. Von Mises stress distribution, symmetry plan XZ

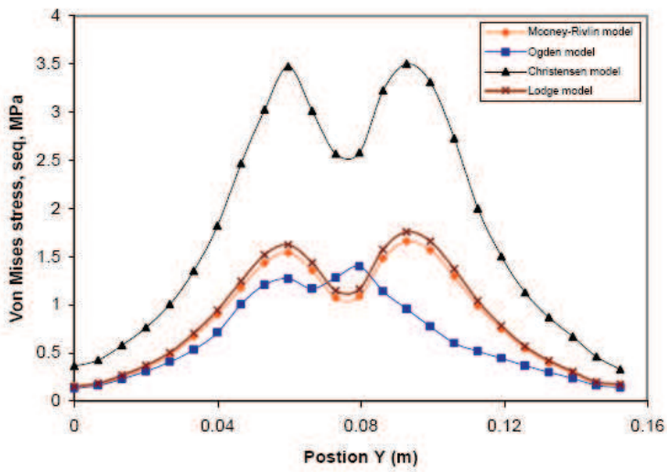

Fig. 11. Von Mises stress distribution, symmetry plan YZ

However numerical calculation shows that there is a difference, not very significant, in the thicknesses distribution (figures 8-9). However, this error can be improved perhaps, either by refining the grid, but at the detriment of a higher computing time, or by improving the technique of biaxial characterization, by the use of a higher number of air flows, as it was underlined in (Erchiqui & al, 2001).

In thermoforming numerical simulation, the thickness prediction is an important goal but the stress estimation is also helpful for part design. Indeed, the prediction of the residual stress and the shape stability of the part are strongly related to the estimated stress. In this section, the stress prediction obtained from the investigated constitutive models is discussed. The localized thinning effect of the deformed membrane is generally accompanied by the increase in the Cauchy stresses or the true stresses of the material. Figures 10-11 present the final von Mises stresses $\sigma_{eq.}$ distribution, predicted by using different constitutive models, on the XZ and YZ half-planes of symmetry in the thermoformed container. For clarity of presentation, the critical values of the von Mises stresses in side zone (A zone) are presented in Tables 2 and 3. The von Mises stress distribution $\sigma_{eq.}$ on the XZ half-plane exhibits the maximum in side zone and the minimum in center zone (B zone). These values are less significant in the half-plane YZ. A comparative study of the numerical results, obtained from the different constitutive models, shows that there is a significant difference between the Christensen model and the other models, for the von Mises stress. The maximum value is obtained for the Christensen model and the minimal value is obtained for the Mooney-Rivlin model. In the XZ half-plane, for zone A, the difference is 1.98 Mpa and for zone B, it is 1.50 Mpa. On the other hand, the difference between the Lodge and the Mooney-Rivlin models is very small. Finally, the Von Mises stress distribution and the localized thinning effect indicates that material failure due to large deformation induced by inflation is most likely to occur in zone A of the container.

Zone	Stress (MPa)	Christensen model	Lodge model	Ogden model	M. Rivlin model
A	σ_{eq}	4.76	2.78	3.57	2.78
B	σ_{eq}	2.58	1.16	1.35	1.08

Table 2. The critical values of the Von Mises stresses, symmetry half-plane XZ.

Zone	Stress (MPa)	Christensen model	Lodge model	Ogden model	M. Rivlin model
A	σ_{eq}	3.50	1.75	1.40	1.66
B	σ_{eq}	2.56	1.14	1.17	1.07

Table 3. The critical values of the Von Mises stresses, symmetry half-plane XZ.

The simple application example of thermoforming of a hollow thin part made of ABS material, shows the advantage of using the dynamic finite elements method based on a total Lagrangian approach, and of using a load in pressure derived from the thermodynamics law of perfect gases, to simulate the structural behavior of hyperelastic and viscoelastic materials.

9. Conclusion

In this work, we have presented the application of a dynamic finite element approach based on the total lagrangian formulation for simulating the response of isotropic, incompressible thermoplastic materials during thermoforming process. The forming load function is defined in terms of gas flow rate instead of static pressure. The validation of the developed finite element software is performed for an ABS material, in the case of free blowing of a circular membrane subjected to a pressure load distribution. Moreover, we have simulated the thermoforming of a rectangular container made of ABS material and studied the influence of hyperelastic (Ogden, Mooney-Rivlin) and viscoelastic (Lodge, Christensen) constitutive laws on the thickness distribution of this thin part, by varying the air flow loading distribution.

10. References

Christensen, R. M. (1980), *Journal Applied Mechanics*. ASME, Vol.47, pp.762-768

DeLorenzi, H. G. & Nied, H. F. (1991), *Progress in polymer processing*, *Hanser Verlag*, Vol.1, pp.117-171

Dennis, J. E.; Schnabel, R. B. (1983), Numerical Methods for Unconstrained Optimization and Nonlinear Equations, Prentice-Hall, Englewood Cliffs

Derdouri, A.; Erchiqui, F.; Bendada, H & Verron, E. (2000), Viscoelastic Behaviour of Polymer Membranes under Inflation, *XIII International Congress on Rheology*, pp.394-396, Cambridge

Erchiqui, F. (2008), *Journal of Reinforced plastics and composites*, Vol.27, No.5, pp.487-505

Erchiqui, F.; Derdouri, A.; Gakwaya, A. & Verron, E. (2001), *Entropie*, 235/236, pp.118-125

Joye, D. D.; Poehlein, G. W. & Denson, C. D. (1972), *Transactions of the Society of Rheology*, Vol.16, pp.421-445

Khayat, R. E.; Derdouri, A. & Garcia-Réjon, A. (1992), *International Journal of Solids and Structures*, Vol.29, No.1, pp.69-87

Landau, D. L. & Lifshitz, E. M. (1984). Cours de Physique Théorique, Tome V, Physique Statistique, Éditions MIR, Moscou

Lapidus, L. & Pinder, G. F. (1982), Numerical solution of partial differential equations in science and engineering, John Wiley & Sons, New-Yorkk, NY

Laroche, D. & Erchiqui, F. (2000), *Journal of Reinforced plastics and composites*, Vol.19, No.3, pp.231-239

Laroche, D. & Erchiqui, F. (1998). *Simulation of materials processing: Theory, methods and applications*. Huétink & Baaijens (eds), Rotterdam: Balkema, ISBN 90 5410 970 X, pp.483-488

Levenberg, K. (1944), An Algorithm for Least-Squares Estimation of Nonlinear Parameters, *Quarterly of Applied Mathematics*, Vol.**2**, pp.164-168

Lodge, A. S. (1964), *Elastic liquids*. Academic Press, London

Marquardt, S. (1963), An Algorithm for Least-Squares Estimation of Nonlinear Parameters, *SIAM Journal on applied Mathematics*, Vol.11, pp.431-441

Ogden, R. W. (1972), Large Deformation Isotropic Elasticity - On the Correlation of Theory and Experiment for for Incompressible Rubberlike Solids, *Proceedings of the Royal Society of London A.*, A326, pp.565-565

Rivlin, R. S. (1948), Some topics in finite elasticity I. Fundamental concepts, *Philosophical Transactions of the Royal Society* A, A240, pp.459-490

Verron, E.; Marckmann, J & Peseux, B. (2001), *International Journal for Numerical Methods in Engineering*, Vol.50, No.5, pp. 1233-1251

IntechOpen

Finite Element Analysis

Edited by David Moratal

ISBN 978-953-307-123-7

Hard cover, 688 pages

Publisher Sciyo

Published online 17, August, 2010

Published in print edition August, 2010

Finite element analysis is an engineering method for the numerical analysis of complex structures. This book provides a bird's eye view on this very broad matter through 27 original and innovative research studies exhibiting various investigation directions. Through its chapters the reader will have access to works related to Biomedical Engineering, Materials Engineering, Process Analysis and Civil Engineering. The text is addressed not only to researchers, but also to professional engineers, engineering lecturers and students seeking to gain a better understanding of where Finite Element Analysis stands today.

InTech Europe

University Campus STeP Ri
Slavka Krautzeka 83/A
51000 Rijeka, Croatia
Phone: +385 (51) 770 447
Fax: +385 (51) 686 166
www.intechopen.com

InTech China

Unit 405, Office Block, Hotel Equatorial Shanghai
No.65, Yan An Road (West), Shanghai, 200040, China
中国上海市延安西路65号上海国际贵都大饭店办公楼405单元
Phone: +86-21-62489820
Fax: +86-21-62489821

IntechOpen